Activity, Folding, Misfolding, and Aggregation *in Vitro* of the Naturally Occurring Human Tissue Factor Mutant R200W†

Jimmy Wiréhn,‡ Karin Carlsson,‡ Anna Herland,§ Egon Persson,|| Uno Carlsson,‡ Magdalena Svensson,‡ and Per Hammarström*,‡

IFM-Departments of Chemistry and Applied Physics, Linköping University, 581 83 Linköping, Sweden, and Haemostasis Biochemistry, Novo Nordisk A/S, Novo Nordisk Park, 2760 Måløv, Denmark

Received December 13, 2004; Revised Manuscript Received March 17, 2005

ABSTRACT: Tissue factor (TF), a small transmembrane receptor, binds factor VIIa (FVIIa), and the formed complex initiates blood coagulation by proteolytic activation of substrate factors IX and X. A naturally occurring mutation in the human TF gene was recently reported, where a single-base substitution results in an R200W mutation in the TF extracellular domain [Zawadzki, C., Preudhomme, C., Gavériaux, V., Amouyel, P., and Jude, B. (2002) *Thromb. Haemost. 87*, 540−541]. This mutation appears to be associated with low monocyte TF expression and may protect against thrombosis but has not been associated with any pathological condition, and individuals who present the heterozygous trait appear healthy. Here, we report the activity, folding, and aggregation behavior of the R200W mutant of the 219-residue soluble extracellular domain of TF (sTF_{R200W}) compared to that of the wild-type protein (sTF_{wt}). No differences in stability or FVIIa cofactor activity but an impaired ability to promote FX activation at physiological conditions between the sTF_{R200W} mutant and sTF_{wt} were evident. Increased binding of 1-anilino-8-naphthalene-sulfonic acid (ANS) to sTF_{R200W} indicated a population of partially folded intermediates during denaturation. sTF_{R200W} showed a dramatically increased propensity for aggregate formation compared to sTF_{wt} at mildly acidic pHs, with an increased rate of aggregation during conditions, promoting the intermediate state. The lowered pH resistance could explain the loss of sTF_{R200W} *in vivo* because of aggregation of the mutant. The intrinsic structure of the sTF aggregates appears reminiscent of amyloid fibrils, as revealed by thioflavin T fluorescence, atomic force microscopy, and transmission electron microscopy. We conclude that the lowered activity for FX activation and the propensity of the mutant protein to misfold and aggregate will both contribute to decreased coagulation activity in TF_{R200W} carriers, which could protect from thrombotic disease.

In the blood coagulation system, proteases are dependent on protein cofactors to improve proteolytic function and direct macromolecular substrate specificity. Blood coagulation is initiated by the cofactor−enzyme complex of tissue factor (TF) and coagulation factor VIIa (FVIIa).[1] The complex ensures normal haemostasis but is also involved in the pathogenesis of different disease processes, including septic shock, thrombotic vascular disease, and cancer metastasis (*1*). Normally, TF is a membrane-bound receptor facing the extracellular space. The protein contains three domains: (i) the extracellular domain (residues 1−219), (ii) the hydrophobic transmembrane domain (residues 220−242), and (iii) the cytoplasmic domain (residues 243−263). The extracellular domain of TF, soluble TF (sTF), is composed of two immunoglobulin-like domains. Previous folding studies of sTF_{wt} and single tryptophan mutants of sTF have been reported (*2*).

An R200W mutation found in human TF seems to be associated with low TF expression (*3*). Only subjects heterozygous for this mutation have been found, and thus far, no connection between the mutation and any disease has been found, rather an indication of an opposite, protective effect. One advantage of a lower amount of functional TF could be a reduced risk for thrombosis. The mutation has a frequency of 1% for people without any history of venous thromboembolic (VTE) disease, whereas it has not been found in people with a history of VTE disease (*3*). Screening of subjects with different case histories is necessary to confirm the prevalence of the mutation, its effect on TF expression, and possible clinical relevance (*3*). It has been found that mice expressing low levels of human TF (∼1% of wild-type levels) have a significantly shorter lifespan than wild-type mice, in part because of spontaneous fatal haemorrhages (*4*). Moreover, TF knock-out mice die *in utero* or shortly after birth. Complete TF deficiency has not been found in humans, indicating that TF is essential (*5*).

† This work was supported by grants from the Foundation for Strategic Research (to P.H.), the Wenner-Gren Foundations (to P.H.), the Swedish Research Council (to P.H. and U.C.), and Carl Tryggers Foundation (to P.H.).

* To whom correspondence should be addressed. Telephone: +46-13-285690. Fax: +46-13-281399. E-mail: perha@ifm.liu.se.

‡ IFM-Department of Chemistry, Linköping University.

§ IFM-Department of Applied Physics, Linköping University.

|| Haemostasis Biochemistry, Novo Nordisk A/S.

[1] Abbreviations: ANS, 1-anilino-8-naphthalene-sulfonic acid; FVIIa, factor VIIa; FX(a), (activated) factor X; GuHCl, guanidine hydrochloride; sTF_{wt}, soluble tissue factor wild type; sTF_{R200W}, soluble tissue factor containing an Arg to Trp mutation in position 200; ThT, thioflavin T.

10.1021/bi047388l CCC: $30.25
Published on Web 04/13/2005

Why the TF_{R200W} mutant is expressed at a lower level is not known. Plausible explanations include misfolding of the protein, aggregation, mislocalization, and degradation. In the cell, protein folding occurs in the cytoplasm or within the secretory pathway. ATP-dependent chaperones collaborate to give a polypeptide chain several opportunities to fold. If folding is unsuccessful, the polypeptide chain is directed to the proteasome for degradation. Aberrant folding inducing loss of function, and degradation of the misfolded protein causes several diseases. Examples are the heritable diseases cystic fibrosis and α1-antitrypsin deficiency. Another category of misfolding diseases are caused by the aggregation of misfolded proteins outside the cell, away from the intracellular control system. The amyloidoses are the major representatives of these disorders, where aggregation is associated with the appearance of a toxic function (*6*). A number of globular proteins with diverse sequences, not currently associated with a protein folding disease, can undergo aggregation *in vitro* into fibrils found in the amyloidoses (*7*). Amyloid fibrils are just one form of aggregate, which is unique in its highly organized hydrogen-bonded structure. This structure gives a kinetic stability, allowing a progressive accumulation of deposits in the tissue.

Here, we report the folding and aggregation behavior of the sTF_{R200W} mutant compared to that of sTF_{wt}. Studies were performed *in vitro* on the extracellular domain of TF where the R200W mutation is located, allowing detailed mechanistic studies of folding, misfolding, and aggregation. Despite indistinguishable stability under physiological conditions of the mutant and wild-type proteins, several important clues are revealed in this study regarding the misfolding and aggregation propensity of the mutant that might explain why it is lost *in vivo*. Our data also provide a possible intriguing link between TF and the amyloidoses.

EXPERIMENTAL PROCEDURES

Chemicals. Thioflavin T (ThT) and 1-anilino-8-naphthalenesulfonic acid (ANS) were obtained from Sigma. ThT was recrystallized prior to use. All other chemicals used were of analytical grade.

Expression and Purification of sTF. sTF_{wt} and sTF_{R200W} were expressed in *Escherichia coli* and purified with anion-exchange chromatography (Q Sepharose Fast Flow) and, optionally, affinity chromatography on a column of immobilized FVIIa as described previously (*8*). The protein concentrations were calculated from absorption measurements using $\epsilon_{280nm} = 37\,440\ M^{-1}\ cm^{-1}$ for sTF_{wt} and $\epsilon_{280nm} = 43\,130\ M^{-1}\ cm^{-1}$ for sTF_{R200W} (calculated value with a contribution of $5690\ M^{-1}\ cm^{-1}$ for one additional tryptophan) (*9*). A Hitachi U-2000 spectrophotometer was used for light absorption measurements.

Activity and Apparent K_d Determinations. The cofactor activity of sTF_{wt} and sTF_{R200W}, after FVIIa affinity chromatography, and their affinity for FVIIa were estimated by the ability to stimulate the amidolytic activity of FVIIa as described earlier (*10*), except that the FVIIa and sTF concentrations were 1 and 2−256 nM, respectively. The K_d values were calculated from the titration curves, and the calculated maximal activity was used as a measure of cofactor activity. The relative abilities of sTF_{wt} and sTF_{R200W} to promote FVIIa-catalyzed activation of FX in solution (without phospholipid) were assessed by mixing 5 nM FVIIa with 200 nM sTF variant (to ensure saturation of FVIIa) and 0.2−4.8 μM FX for 20 min. Only low nanomolar concentrations of FXa were generated during the assay, and the generation was linear with time. FXa generation was stopped by adding excess EDTA and quantified using 0.5 mM S-2765 (Chromogenix, Mölndal, Sweden). Amidolytic and proteolytic activity measurements were performed 3 times.

Intrinsic Fluorescence Measurements. The intrinsic Trp fluorescence was measured for sTF_{wt} and sTF_{R200W}, with a protein concentration of 9.6 μM in Na-borate buffer. Spectra were recorded at 23 °C for protein purified with and without FVIIa affinity chromatography. The excitation wavelength was 295 nm, and three accumulative emission spectra, in the wavelength region of 305−450 nm, were recorded. Slits for excitation and emission were set to 5 nm. A Hitachi F-4500 fluorescence spectrophotometer, equipped with a thermostated cell, was used to record all fluorescence spectra.

Stability Measurements: (i) Unfolding. The protein (2 μM) was incubated overnight in various concentrations of GuHCl (0−4 M) containing 50 mM Tris-HCl at pH 7.5. The unfolding of the protein could be monitored by the intrinsic tryptophan fluorescence. Spectra were recorded at 23 °C in a 1-cm quartz cuvette. The excitation wavelength was 295 nm, and for each measurement, three emission spectra were recorded in the wavelength region of 305−450 nm. For both excitation and emission, 5-nm slits were used. Wavelength and intensity of maximum emission were registered.

(ii) Refolding. The protein (20 μM) was denatured for 24 h in 4 M GuHCl. Refolding was performed by a 10-fold dilution of the unfolded protein solution in various concentrations of GuHCl (0.4−3 M) and a final protein concentration of 2 μM. All solutions were buffered with 50 mM Tris-HCl at pH 7.5. The samples were incubated overnight, and then the intrinsic tryptophan fluorescence was measured under the same conditions as for the stability measurements described above.

The unfolding transition curve (Trp maximal emission shift versus the GuHCl concentration) was fitted to a single transition. The Gibbs free energy of folding in the absence of denaturant (ΔG^{H_2O}) was determined through linear extrapolation to 0 M GuHCl using the formula $\Delta G = \Delta G^{H_2O} - m[\text{GuHCl}]$ (*11*).

ANS Fluorescence. The samples from stability and refolding measurements (see above) were also used for ANS binding experiments. A total of 3.6 μL of ANS, from a 10 mM stock solution, was mixed with 900 μL of each sample giving a final concentration of 40 μM ANS and 2 μM sTF. The ANS fluorescence spectra were measured at 23 °C with a 1-cm quartz cuvette. The excitation wavelength was set to 360 nm, and three emission spectra were recorded in the wavelength region of 380−600 nm for each sample. The excitation and emission slits were set to 10 nm. The intensity at 480 nm for the ANS fluorescence emission was registered.

Aggregation Studies. To monitor the pH-dependent aggregation profile of sTF, a sample series of varying pHs was set up. For this purpose, 0.1 M Na-citrate buffers, in the range of pH 3−6, were used. sTF_{wt} and sTF_{R200W} were dialyzed against dH_2O. Samples were prepared by mixing 250 μL of protein solution (0.4 mg/mL, 16 μM) with 250 μL of citrate buffer and then incubated for 4 days at 37 °C in a stagnant assay with a final protein concentration of 0.2 mg/mL.

To quantify the amount of aggregated protein formed, a spectrophotometer (Hitachi U-2000) was used for light-scattering and absorption measurements. A wavelength scan, from 250 to 500 nm, was performed (after mixing the solution thoroughly). The optical densities at 330 and 400 nm were recorded. The samples were then centrifuged for 10 min at 10 000 rpm. Absorption at 280 nm was then registered on the supernatant and was used as a measure of remaining soluble protein monomers. The higher absorbance by the sTF_{R200W} mutant compared to sTF_{wt} because of the additional tryptophan in the mutant was adjusted in the concentration determination.

Kinetic measurements were performed at pH 4.0 and 5.0. A total of 500 μL of protein (0.4 mg/mL, 16 μM in dH_2O) was mixed with 500 μL of 0.1 M Na-citrate buffer, providing the desired pH, in a sealed plastic cuvette. The optical density at 330 and 400 nm (light scattering) was recorded. The cuvette was then placed in a water bath at 37 °C. The samples were rigorously mixed using a vortex for 3 s before each measurement. Wavelength scans were performed continuously the first day followed by a few scans per day for another 3 days. In the same way, measurements were performed in the presence of 0.25 M GuHCl at pH 5.0.

ThT Fluorescence. To monitor possible amyloid fibril formation during aggregation of sTF at different pH values, the fluorescent dye ThT was used. Aggregation samples were centrifuged for 10 min at 13 000 rpm, and the supernatant was removed, leaving ~30 μL of pellet. The pellet was mixed with 470 μL of ThT assay solution [5.3 μM ThT and 53 mM Tris-HCl (pH 7.5)]. This gave a final protein concentration of ~8 μM (if the pellet contained all of the protein). A 1-cm quartz cuvette was used, and measurements were carried out at 23 °C. The excitation wavelength for ThT was set to 440 nm, and one scan in the region 455−600 nm was recorded. The excitation slit was set to 5 nm, and the emission slit was set to 10 nm. Intensity of the ThT fluorescence emission at 482 nm was registered. Quantification of the amount of aggregated sTF protein in the ThT assay samples was done by centrifugation of the samples for 10 min at 13 000 rpm. The supernatant was removed, and the pellet was lyophilized. The lyophilized pellet was dissolved in 50 μL of 8 M GuHCl, and the amount of protein was determined by the Bradford assay (Pierce) (15 μL of sTF aggregates and 185 μL of Bradford assay solution) using a 96-well absorbance plate reader to determine the absorbance at 590 nm. The amount of protein was quantified using a sTF standard curve with a known protein concentration.

As references for ThT fluorescence, amyloid fibrils of human transthyretin (TTR) and bovine insulin (BI) were generated. Amyloid fibrils of TTR (A-TTR) were generated by incubation of 0.20 mg/mL TTR (=14 μM on a monomer basis) in 100 mM sodium acetate, 150 mM KCl, and 1 mM EDTA (pH 4.4) for 96 h (37 °C) (*12*, *13*). The amount of aggregated protein was determined by centrifugation for 10 min at 13 000 rpm, whereafter the concentration of free monomer was determined by A_{280} of the supernatant. The supernatant was removed leaving ~30 μL of pellet. In this TTR aggregation assay, 70% of the protein precipitates, i.e., 0.14 mg/mL into A-TTR. The pellet was mixed with 470 μL of ThT assay solution. Amyloid fibrils of BI (A-BI) were generated by incubation of 2.77 mg/mL BI (=0.50 mM) in 25 mM HCl for 14 h (65 °C) (*14*), which results in complete conversion of BI into amyloid fibrils. Aliquots from the A-BI fibril solution were mixed with the ThT assay solution to a final concentration of 0.14 mg/mL. The ThT fluorescence intensity was normalized to the mass of aggregated protein: sTF_{wt} (0.077 mg/mL), $sTFR_{200W}$ (0.12 mg/mL), A-TTR (0.14 mg/mL), and A-BI (0.14 mg/mL).

Table 1: Binding to FVIIa and Activity of the Complex

sample	activity (% of sTF_{wt})[a]	K_d (nM)[b]
sTF_{wt}	100	2.9 ± 0.3
sTF_{R200W}	96	4.0 ± 0.3

[a] Cofactor activity, measured as the maximal enhancement of amidolytic activity. [b] K_d for FVIIa complex formation.

Transmission Electron Microscopy (TEM). Aggregation samples of sTF_{wt} and sTF_{R200W} incubated for 4 days at 37 °C at pH 4.0 in a stagnant assay with a final protein concentration of 0.2 mg/mL were analyzed by TEM. Aliquots (5 μL) of the sample were applied to carbon-coated grids (Ted Pella, Inc.) for 2 min. The grids were washed with 5 μL of water and were negatively stained with uranyl acetate in water 2% (wt/vol) for 20 s. The grids were air-dried overnight before examined in a Phillips EM400 transmission electron microscope used at an accelerating voltage of 120 kV.

Atomic Force Microscopy (AFM). AFM imaging was performed in tapping mode on a SFM-Nanoscope III, Digital Instruments, with a J-scanner. Cantilevers for tapping mode were obtained from NT-MDT. For the AFM observations, 10 μL of aggregation samples (sTF_{wt} and sTF_{R200W} incubated for 4 days at 37 °C at pH 4.0 in a stagnant assay with a final protein concentration of 0.2 mg/mL) were applied to a hydrophobic silicon (100) surface coated with a monolayer of dichlorodimethylsilane, incubated for 2 min, and excess protein was removed by extensive rinsing in deionized water followed by drying using pressurized N_2.

RESULTS AND DISCUSSION

Activity and Apparent K_d Determinations. Samples of sTF_{wt} and sTF_{R200W} were analyzed to determine the K_d value for FVIIa binding and the FVIIa cofactor activity. The results are presented in Table 1. The sTF_{wt} and the mutant are very similar in their interaction with FVIIa, which is not surprising given that residue 200 is located on the opposite side of the FVIIa binding surface, i.e., closer to the suggested FX binding surface. Measurements performed with the FVIIa/sTF_{R200W} complex as a FX activator showed that it activated FX at a maximal rate corresponding to 43 ± 6% of that of the FVIIa/sTF_{wt} complex. These results on FX activation are in line with those obtained with other sTF variants, with substitutions at position 200, namely, sTF_{R200C} (*10*) and $sTF_{N199A/R200A}$ (*15*), all displaying a 2−4-fold reduction compared with wild-type sTF. In these cited studies, residue 200 was shown to be involved in FX binding by the use of site-directed labeling (*10*) and alanine scanning (*15*). The importance of residue 200 is also supported by modeling studies (*16*, *17*). Taken together, residue 200 is located in an area on the TF surface involved in the exosite-mediated recognition of FX (and FIX) by the FVIIa/TF complex. However, the K_m values of FVIIa/sTF_{wt} and FVIIa/sTF_{R200W} for FX were both between 2 and 3 μM and not significantly different. Hence, the sTF_{R200C} variant resembles sTF_{R200W} in

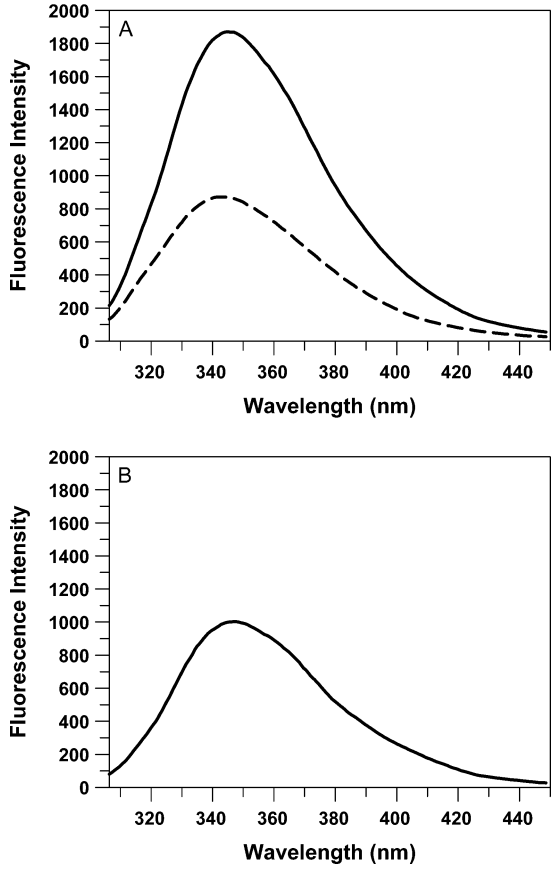

FIGURE 1: Comparison of intrinsic Trp fluorescence of sTF_{R200W} and sTF_{wt}. (A) sTF_{wt} (- - -) and sTF_{R200W} (—). (B) Difference spectrum between sTF_{R200W} and sTF_{wt}.

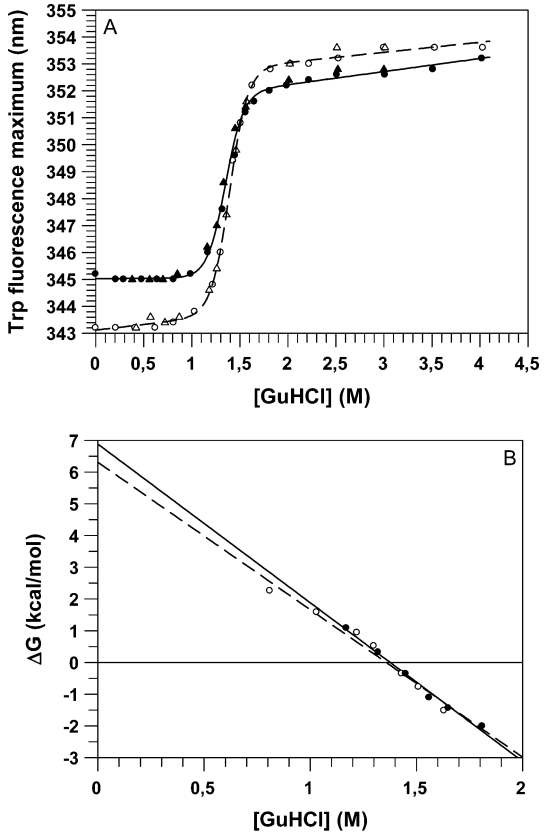

FIGURE 2: Stability of sTF_{R200W} and sTF_{wt} toward GuHCl denaturation. (A) Global unfolding of sTF_{wt} (○) and sTF_{R200W} (●) and global refolding of sTF_{wt} (△) and sTF_{R200W} (▲), measured by intrinsic Trp fluorescence. (B) Gibbs free energy of unfolding (ΔG) as a function of [GuHCl] for sTF_{wt} (○, - - -) and sTF_{R200W} (●, —). Denaturation was performed at pH 7.5.

that the amidolytic FVIIa cofactor activity was normal despite a reduction in FX activation rate. The substitution of a bulky, hydrophobic Trp side chain for the positively charged Arg in position 200 definitely has the potential to affect the binding and presentation of FX. This may very well also attenuate FX activation by FVIIa/TF_{R200W} on a cell surface.

Trp Fluorescence Spectra. sTF contains four Trp residues distributed throughout the structure, out of which essentially only two contribute to the intrinsic Trp fluorescence intensity in the native protein (W14, 23% and W45, 73%) (*18*). In Figure 1A, the intrinsic Trp fluorescence spectra of sTF_{wt} and sTF_{R200W} are shown. The additional Trp of the mutant gives a significant contribution to the intensity of fluorescence emission, and the spectrum is red-shifted from 343 nm for sTF_{wt} to 345 nm for the mutant. A difference spectrum between sTF_{R200W} and sTF_{wt} spectra is shown in Figure 1B, showing a Trp fluorescence peak at 347 nm, indicating that Trp 200 is located in a rather polar environment, at the surface of the protein, consistent with the crystal structure (*19*−*21*). All tryptophans are expected to fluoresce in the unfolded protein providing a red-shifted fluorescence spectrum because of exposure to the solvent compared to the native sTF_{wt} protein, which shows blue-shifted fluorescence from the partially buried W14 and W45. Thus, we used Trp fluorescence as a probe for folding and unfolding of both the wild type and mutant to provide a parameter of global conformational change. Previously, near-UV CD has been used in our laboratory for folding studies of sTF (*2*).

Folding and Stability. After incubation at various concentrations of GuHCl, an unfolding transition curve was obtained by plotting the wavelength of maximum Trp fluorescence versus the GuHCl concentration (Figure 2A). These unfolding measurements showed no significant differences in stability between the sTF_{wt} protein and the sTF_{R200W} mutant; if anything, the mutant was slightly more stable. The midpoints of denaturation were 1.35 and 1.37 M GuHCl for sTF_{wt} and sTF_{R200W}, respectively (Figure 2A), and the Gibbs free energy of folding (ΔG^{H_2O}) was −6.3 kcal/mol for sTF_{wt} and −6.9 kcal/mol for sTF_{R200W} (Figure 2B). The denaturation process is completely reversible, because refolding of unfolded sTF_{wt} and sTF_{R200W} gave results that were superimposable on the unfolding curves (Figure 2A).

ANS Fluorescence Indicates a Populated Intermediate. ANS is a hydrophobic dye that binds to exposed hydrophobic regions of partially folded proteins, leading to an increase in ANS fluorescence intensity (*22*). Figure 3 shows ANS fluorescence, at 480 nm, for various concentrations of GuHCl. There is an obvious increase in fluorescence intensity during unfolding, indicating the presence of a population of an intermediate, possibly of molten-globule type, during unfolding. The interesting result was the significant increase in fluorescence for ANS when binding to sTF_{R200W} compared to sTF_{wt}. This suggests either (i) that the partly denatured (intermediate) state of sTF_{R200W} has a structure with more exposed hydrophobic regions than the sTF_{wt} protein or (ii) that the sTF_{R200W} mutant populates the intermediate to a larger degree than sTF_{wt}. We cannot directly distinguish between these two possibilities. However, there was no obvious difference in the *m* values according to the slopes

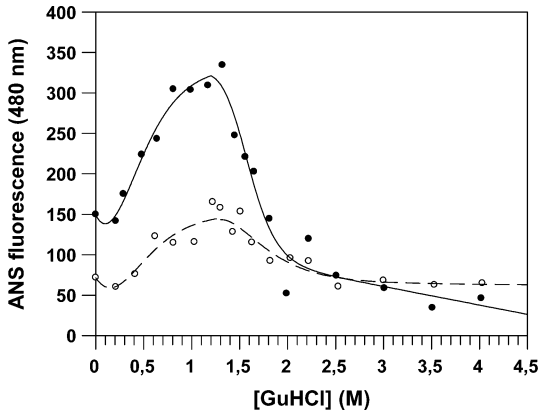

FIGURE 3: ANS binding to sTF_{R200W} and sTF_{wt} during unfolding. ANS fluorescence at 480 nm in the presence of sTF_{wt} (○, - - -) and sTF_{R200W} (●, —) incubated at various concentrations of GuHCl (pH 7.5). Lines were drawn to guide the eye.

of the free energy versus denaturant concentration curves for sTF_{R200W} and sTF_{wt} (Figure 2B), which would favor the second alternative, i.e., increased population of intermediates, rather than exposed hydrophobic surfaces, because *m* values are believed to reflect the degree of exposed surface area (*23*).

Aggregation Studies. Protein aggregation was monitored by turbidity measurements and loss of soluble protein by absorption spectrophotometry. The turbidity was estimated by absorbance measurements at 330 and 400 nm by monitoring the amount of scattered light of formed aggregates at different pHs (parts A and B of Figure 4). The sTF_{R200W} mutant showed aggregate formation in the pH range of 3.6−5.7, with a maximum amount of scattering of around pH 4.1. Comparing sTF_{wt} and sTF_{R200W} demonstrates that also sTF_{wt} aggregates in the same pH range (pH 3.6−5.7) but exhibits maximal scattering at pH 4.0, i.e., at a slightly lower pH than the mutant. The most significant difference, however, is that the sTF_{R200W} mutant forms aggregates to a much higher degree than the sTF_{wt} protein. One explanation could be the location of the mutation at the surface of the protein. The rather apolar tryptophan side chain will contribute to a more hydrophobic protein surface, whereas the arginine present in position 200 in sTF_{wt}, with a positively charged side chain, could work as an intermolecular gatekeeper preventing aggregation through charge−charge repulsion.

In addition to turbidity measurements, quantification of insoluble protein was complemented by loss-of-monomer measurements. In this experiment, we used absorbance measurements at 280 nm of the supernatant from centrifuged aggregation samples (Figure 4C). Determination of remaining soluble protein, following removal of the precipitated protein, showed a shift toward lower pH compared to turbidity measurements. The solubility minimum was at pH 3.75 and 3.6 for sTF_{R200W} and sTF_{wt}, respectively (Figure 4C). Despite the fact that the solubility is lower at more acidic pH, aggregates formed at pH 4.0−4.1 scatter light more efficiently than aggregates formed at pH 3.6−3.9, indicating that aggregates formed at pH 4.0−4.1 are larger.

Aggregate Morphology. To obtain more information of the formed aggregates, ThT was used to investigate whether amyloid-like fibrils were formed during aggregation of the protein. When ThT binds to amyloid fibrils, it results in a

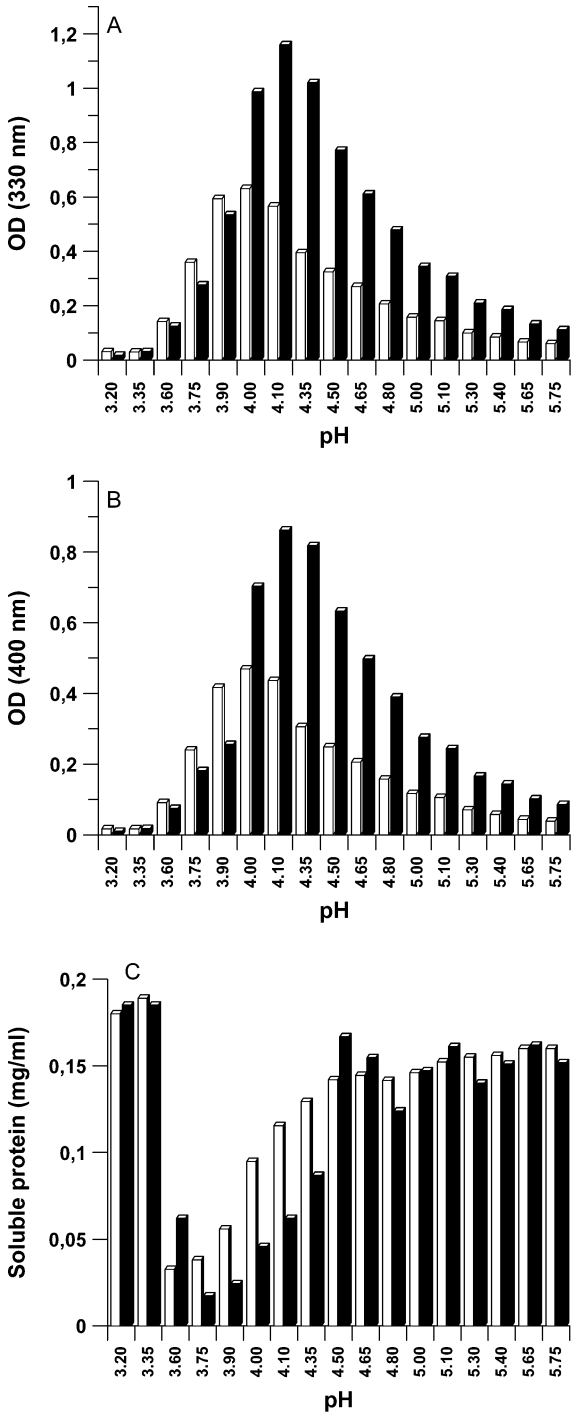

FIGURE 4: Aggregation studies of sTF_{R200W} and sTF_{wt}. Light scattering measured by optical density (OD) of sTF aggregates at (A) 330 nm and (B) 400 nm, at various pH values. (C) Nonaggregated soluble protein following centrifugation quantified by absorbance at 280 nm. All data were recorded from stagnant aggregation assays [8 μM protein (0.2 mg/mL), 37 °C, 4 days]. White bars represent sTF_{wt}, and black bars represent sTF_{R200W}.

major increase in fluorescence intensity, at 482 nm (*24*). The fluorescence intensity of ThT bound to pelleted protein aggregates formed at different pH values (protein incubated 4 days at 37 °C) is shown in Figure 5A. There is a strong increase in ThT fluorescence showing peaks at pH 4.1 and 3.75 for sTF_{R200W} and sTF_{wt}, respectively. For sTF_{R200W}, this agrees well with the light-scattering measurements, which showed that the largest aggregates were formed at pH 4.1 (parts A and B of Figure 4), whereas sTF_{wt} shows a pH

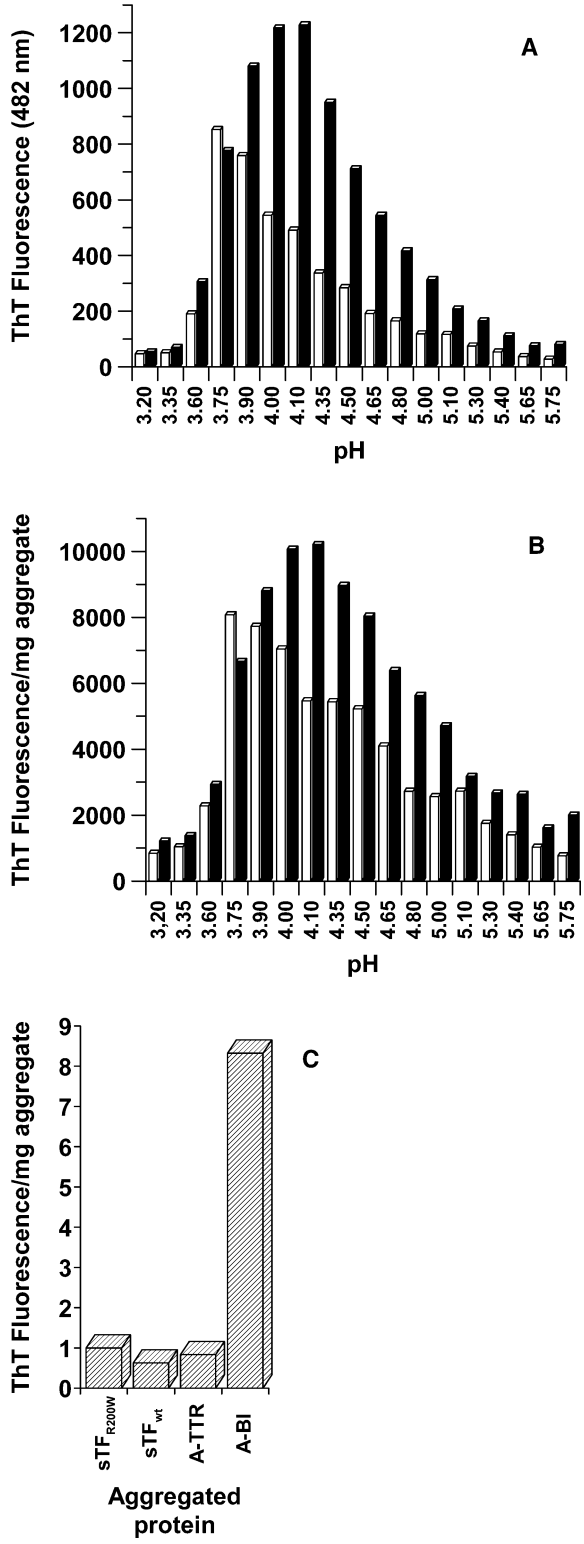

FIGURE 5: ThT binding to pelleted sTF aggregates. Amyloid-like aggregate formation monitored by ThT binding to aggregates formed by sTF_{wt} (white bars) and sTF_{R200W} (black bars) at different pH values [8 μM protein (0.2 mg/mL), 37 °C, 4 days]. (A) Total measured ThT fluorescence intensity at 482 nm. (B) Total ThT fluorescence intensity at 482 nm normalized to the mass (mg) of formed aggregates. (C) Total ThT fluorescence intensity at 482 nm normalized to the mass (mg) of sTF_{R200W} and sTF_{wt} aggregates formed during incubation at pH 4.0. As references, the ThT fluorescence of the sTF aggregates are compared with amyloid fibrils of transthyretin (A-TTR) and bovine insulin (A-BI). The intensity of sTF_{R200W} was set to 1.0.

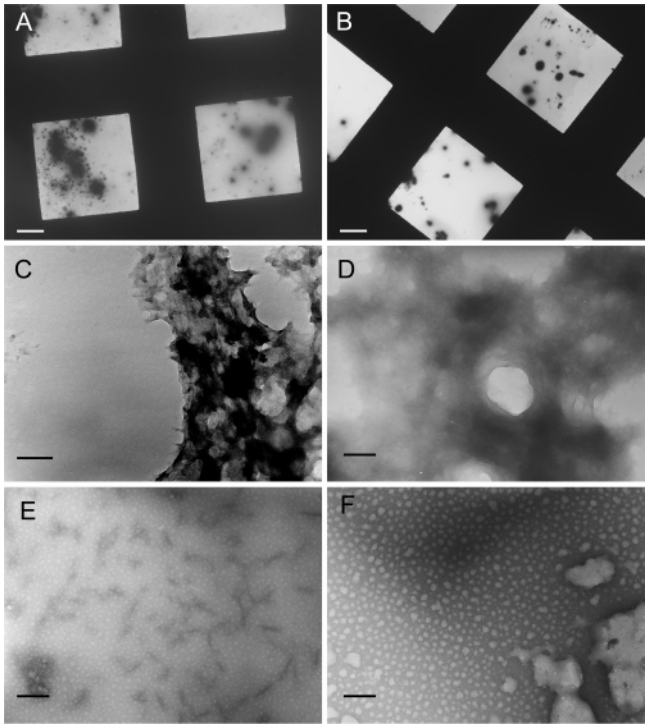

FIGURE 6: Aggregate morphology by TEM. TEM micrographs of sTF_{R200W} (left panel) (A, C, and E) and sTF_{wt} (right panel) (B, D, and F) aggregates formed during incubation at pH 4.0. A and B were taken at 600-fold magnification. Here, the scale bar indicates 10 μm. C−F were taken at 36 000-fold magnification, and the scale bar indicates 200 nm.

optimum for ThT binding between the pH for the turbidity maximum and the solubility minimum. The increased ThT fluorescence for the sTF_{R200W} mutant compared with that of sTF_{wt} is well in accordance with the turbidity and solubility data, showing that the mutant aggregates more extensively than sTF_{wt}. To get a more quantitative comparison, the ThT fluorescence intensity was normalized to the mass of aggregated protein (Figure 5B). Still, the mutant fluoresced more than the wild type, although the difference was somewhat less pronounced. As references for the ThT assay, amyloid fibrils of human transthyretin, A-TTR, and bovine insulin, A-BI, were analyzed using the same assay. The ThT fluorescence intensity was normalized to the mass of formed fibrils. The comparison showed that ThT bound to sTF_{R200W} aggregates fluoresces even slightly more than A-TTR amyloid fibrils, which in turn fluoresce 8-fold less than A-BI (Figure 5C). These data indicate that the sTF aggregates show ThT fluorescence properties comparable to known amyloid fibrils.

Aggregates of the sTF mutant and wild type formed at pH 4.0 were studied by by TEM. Figure 6 shows electron micrographs taken at different degrees of magnification. In parts A and B of Figure 6, overview pictures of the EM grids show the massive precipitation of sTF_{R200W} and sTF_{wt} and, as expected, the mutant shows larger depositions of aggregates. At higher magnification, two different regions of the same sample are shown. In parts C and D of Figure 6, showing the most representative areas, it is evident that the formed aggregates were massively clumped and displayed some fibrillar texture. Detailed morphology of the aggregates was very hard to elucidate because of the severe clustering, but the ThT binding indicates an intrinsic structure reminding

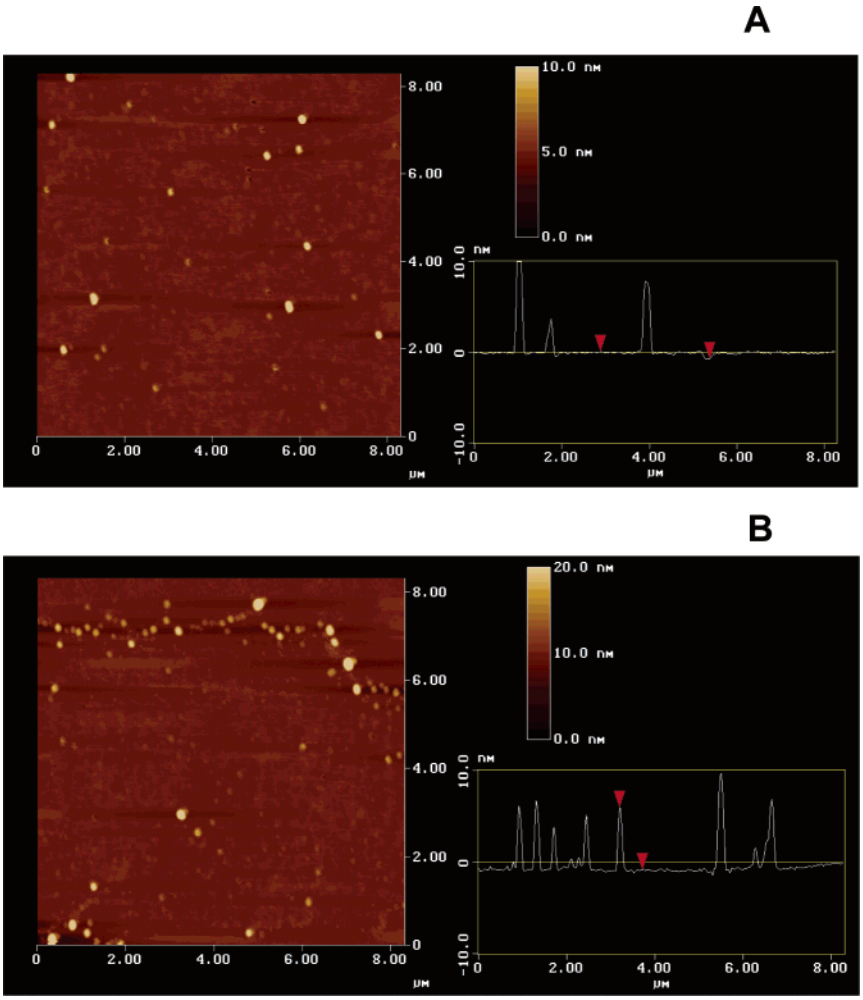

FIGURE 7: Aggregate thickness by AFM. AFM micrographs of sTF_{R200W} (A) and sTF_{wt} (B) aggregates formed during incubation at pH 4.0. AFM height mode micrographs were taken in tapping mode shown in the main picture. A scan to analyze the height distribution of the aggregates is shown in the bottom right part of the images.

of amyloid fibrils or protofibrils. Micrographs showing less crowded areas of sTF_{R200W} and sTF_{wt} aggregates are shown in parts E and F of Figure 6. The mutant sample (Figure 6E) shows the presence of diffuse 100−200 nm long and 10 nm wide fibril-like rods and 5−10 nm wide globular species that appear to be oligomeric assemblies of misfolded sTF_{R200W}. The corresponding area from the sTF_{wt} samples (Figure 6F) shows the presence of 10−30 nm wide globular oligomers. The fibrillar structures found in the mutant sample appear to be absent in the sTF_{wt} sample; however, these species could easily be overlooked by TEM, or they could be associated to the large aggregate clusters (Figure 6D). AFM was employed to obtain height information of the aggregates. Figure 7 shows AFM micrographs of mutant and wild-type aggregates. Here, the method relies on adsorption to the hydrophobic silanized-silicon surface, and the adsorbed aggregates appear clumped in 200−400 nm large clusters. The wild type appears to adsorb more efficiently to the coated surface than the mutant (Figure 7). Height analysis of the large aggregates formed from both misfolded sTF_{wt} and sTF_{R200W} revealed that their average height was in the range of 5−12 nm. This height is within the expected thickness of amyloid fibrils (*25*).

Aggregation Kinetics. Kinetic measurements of aggregate formation are represented in Figure 8, as light scattering at 330 nm over time. Table 2 lists the aggregation rates. The kinetics of sTF_{R200W} and sTF_{wt} aggregation was compared at pH 5.0 and 4.0 (parts A and B of Figure 8). The sTF_{wt} aggregation rate is not affected significantly by the environment. On the other hand, sTF_{R200W} shows a strong correlation of the aggregation rate versus pH. At pH 5.0, sTF_{R200W} and sTF_{wt} aggregate with very similar rates, but at pH 4.0, the rate for sTF_{R200W} is significantly higher. When increased denaturation stress is applied at pH 5.0, by the addition of 0.25 M GuHCl, the aggregation of the mutant is accelerated 3-fold, indicating that when the folding intermediate of sTF_{R200W} is more populated the aggregation rate increases. Increased population of intermediates is well-known to favor aggregation (*26*, *27*).

CONCLUDING REMARKS

The stability of sTF is not affected by the R200W mutation under conditions that are close to the physiological environment, and there is no effect on FVIIa cofactor activity. However, even though sTF_{R200W} stimulates FVIIa normally, as measured using a tripeptidyl FVIIa substrate, the complex with FVIIa exhibits a reduced ability to activate FX. The R200W substitution appears to be an aggregation mutation showing strong pH dependence. sTF_{R200W} aggregates more *in vitro* and more extensively in less acidic environments than the sTF_{wt} protein, showing that sTF_{R200W} is more sensitive to pH changes. This could have an effect *in vivo*

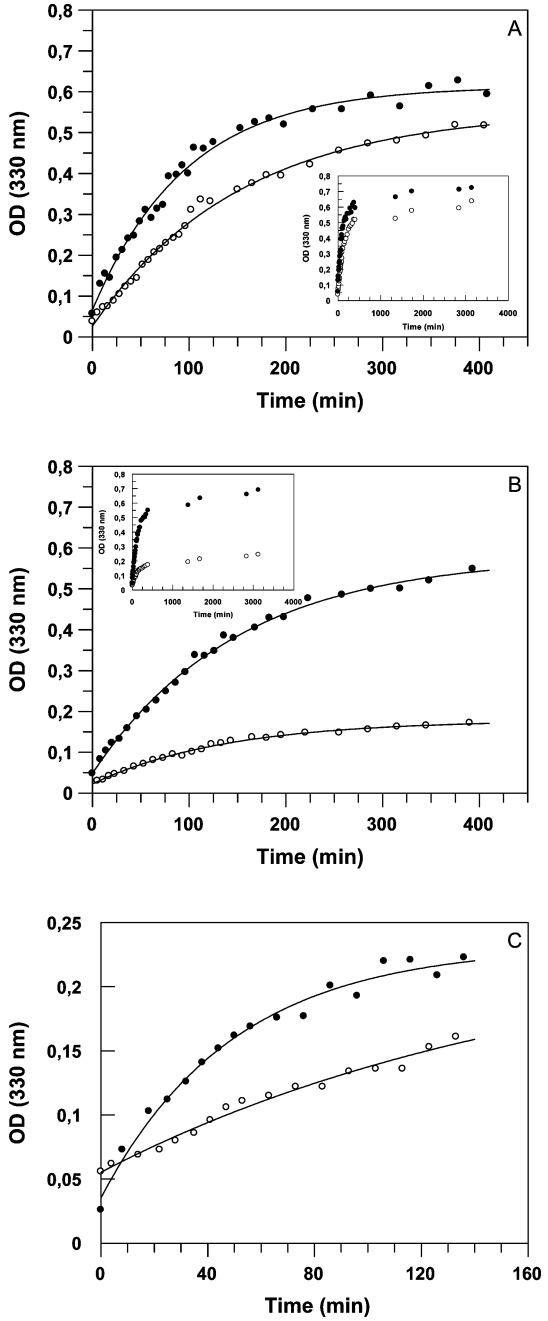

FIGURE 8: Aggregation kinetics of sTF_{R200W} and sTF_{wt}. Time courses of sTF_{wt} (○) and sTF_{R200W} (●) (37 °C, 8 μM) at (A) pH 4.0 and (B) pH 5.0. Insets show traces up to 2 days of aggregation. (C) Aggregation kinetics at pH 5.0 in the presence of 0.25 M GuHCl. The curves were fitted using the single-exponential function $A_{330} = a(1 - e^{-kt}) + b$.

Table 2: Aggregation Kinetics of sTF_{wt} and sTF_{R200W}

sample	k (min^{-1})	$t_{1/2}$ (min)
sTF_{wt} at pH 4.0	0.0065	106
sTF_{wt} at pH 5.0	0.0073	95
sTF_{wt} at pH 5.0 and 0.25 M GuHCl	0.0059	118
sTF_{R200W} at pH 4.0	0.010	67
sTF_{R200W} at pH 5.0	0.0067	104
sTF_{R200W} at pH 5.0 and 0.25 M GuHCl	0.020	34

because of pH differences in various cellular compartments. TF encounters a variety of different pH values *in vivo*, during its transportation from the endoplasmic reticulum (ER) to the final destination at the cell surface. ANS binding and aggregation kinetics showed that sTF_{R200W} populates partially folded hydrophobic intermediate states during folding and denaturation, which could explain the higher tendency of aggregate formation for the mutant. The formed aggregates bind ThT, which has fibrillar structures as revealed by TEM, with the typical amyloid fibril thickness in the range of 5−12 nm as shown by AFM. All of these features indicate an intrinsic structure similar to that of amyloid fibrils. The TF protein is folded into two fibronectin III-like domains of β-sandwich type (*19*−*21*). Interestingly, a domain of fibronectin III has been reported to form amyloid-like fibrils *in vitro* (*28*). Although several proteins forming amyloid fibrils *in vitro* are not associated with human pathology, the β-sandwich proteins transthyretin, β-microglobulin, and immunoglobulin light chain are all associated with human amyloid diseases (*29*). It is appealing to hypothesize what biological implications TF aggregation could have in the *in vivo* context. There is a possible intriguing link between TF and human amyloid disease. The findings in this paper indicate that TF can misfold into amyloid-like aggregates and that TF can be recruited to preformed amyloid fibrils *in vitro* (unpublished data). Recruitment of TF to amyloid fibrils would thereby lower the coagulation activity in a patient suffering from amyloidosis. Interestingly, a well-known side effect of systemic immunoglobulin light-chain (AL) amyloidosis is extensive haemorrhage (*30*). This has been attributed to the loss of FX because of recruitment to preformed amyloid deposits based on activity measurements (*31*). However, recent data have shown that the concentration of FX has increased in systemic AL-amyloidosis patients suffering from haemorrhage, but the amount of active FXa has decreased, rather indicating a loss of FX activation than a loss of the FX protein (*30*). We propose that the abnormal bleedings in systemic AL-amyloidosis could be explained by loss of TF because of recruitment to light-chain amyloid fibrils.

It is important to point out that the carriers of the TF_{R200W} mutant appear healthy, and these carriers seem to have a lowered risk for thrombosis (*3*). Although this conclusion is based on a small number of individuals, this is likely associated with low concentrations of normally folded TF at the cell surface. The missing TF protein has been lost during folding in the ER, transport, or membrane insertion and is likely degraded within the cell. Furthermore, even if TF_{R200W} reaches its target site at the cell membrane, it will still only possess about half the activity of TF_{wt} in activating FX. It is tempting to predict that a carrier of the TF_{R200W} trait would suffer from severe haemorrhage, if struck with systemic AL-amyloidosis.

ACKNOWLEDGMENT

We thank Anette Østergaard for technical assistance.

REFERENCES

1. Ruf, W., Shobe, J., Rao, S. M., Dickinson, C. D., Olson, A., and Edgington T. S. (1999) Importance of factor VIIa Gla-domain residue Arg-36 for recognition of the macromolecular substrate factor X Gla-domain, *Biochemistry 38*, 1957−1966.
2. Andersson, D., Carlsson, U., and Freskgård, P.-O. (2001) Contribution of tryptophan residues to the CD spectrum of the extracellular domain of human tissue factor, *Eur. J. Biochem. 268*, 1118−1128.

3. Zawadzki, C., Preudhomme, C., Gavériaux, V., Amouyel, P., and Jude, B. (2002) The Arg200Trp mutation in the human tissue factor gene, *Thromb. Haemost. 87*, 540−541.
4. Pawlinski, R., Fernandes, A., Kehrle, B., Pedersen, B., Parry, G., Erlich, J., Pyo, R., Gutstein, D., Zhang, J., Castellino, F., et al. (2002) *Proc. Natl. Acad. Sci. U.S.A. 99*, 15333−15338.
5. Hogan, K. A., Weiler, H., and Lord, S. T. (2002) Mouse models in coagulation, *Thromb. Haemost. 87*, 563−574.
6. Cohen, F. E., and Kelly, J. W. (2003) Therapeutic approaches to protein-misfolding diseases, *Nature 426*, 905−909.
7. Selkoe, D. J. (2003) Folding proteins in fatal ways, *Nature 426*, 900−904.
8. Österlund, M., Owenius, R., Carlsson, K., Carlsson, U., Persson, E., Lindgren, M., Freskgård, P.-O., and Svensson, M. (2001) Probing inhibitor-induced conformational changes along the interface between tissue factor and factor VIIa, *Biochemistry 40*, 9324−9328.
9. Gill, S. C., and von Hippel, P. H. (1989) Calculation of protein extinction coefficients from amino acid sequence data, *Anal. Biochem. 182*, 319−326.
10. Carlsson, K., Freskgård, P.-O., Persson, E., Carlsson, U., and Svensson, M. (2003) Probing the interface between factor Xa and tissue factor in the quaternary complex tissue factor-factor VIIa-factor Xa-tissue factor pathway inhibitor, *Eur. J. Biochem. 270*, 2576−2582.
11. Santoro, M. M., and Bolen, D. W. (1988) Unfolding free energy changes determined by the linear extrapolation method. 1. Unfolding of phenylmethanesulfonyl α-chymotrypsin using different denaturants, *Biochemistry 27*, 8063−8068.
12. Lai, Z., Colon, W., and Kelly J. W. (1996) The acid-mediated denaturation pathway of transthyretin yields a conformational intermediate that can self-assemble into amyloid, *Biochemistry 35*, 6470−6482.
13. Hammarström, P., Schneider, F., and Kelly, J. W. (2001) Trans-suppression of misfolding in an amyloid disease, *Science 293*, 2459−2462.
14. Nilsson, K. P., Herland, A., Hammarström, P., and Inganäs, O. (2005) Conjugated polyelectrolytes: Conformation-sensitive optical probes for detection of amyloid fibril formation, *Biochemistry 44*, 3718−3724.
15. Kirchhofer, D., Lipari, M. T., Moran, P., Eigenbrot, C., and Kelley, R. F. (2000) The tissue factor region that interacts with substrates factor IX and factor X, *Biochemistry 39*, 7380−7387.
16. Venkateswarlu, D., Duke, R. E., Perera, L., Darden, T. A., and Pedersen L. G. (2003) An all-atom solution-equilibrated model for human extrinsic blood coagulation complex (sTF-VIIa−Xa): A protein−protein docking and molecular dynamics refinement study, *J. Thromb. Haemost. 1*, 2577−2588.
17. Norledge, B. V., Petrovan, R. J., Ruf, W., and Olson, A. J. (2003) The tissue factor/factor VIIa/factor Xa complex: A model built by docking and site-directed mutagenesis, *Proteins 53*, 640−648.
18. Hasselbacher, C. A., Rusinova, E., Waxman, E., Rusinova, R., Kohanski, R. A., Lam, W., Guha, A., Du, J., Lin, T. C., Polikarpov, I., Boys, C. W. G., Nemerson, Y., Konigsberg, W. H., and Ross, J. B. A. (1995) Environments of the four tryptophans in the extracellular domain of human tissue factor: Comparison of results from absorption and fluorescence difference spectra of tryptophan replacement mutants with the crystal structure of the wild-type protein, *Biophys. J. 69*, 20−29.
19. Harlos, K., Martin, D. M. A, O'Brien, D. P., Jones, E. Y., Stuart, D. I., Polikarpov, I., Miller, A., Tuddenham, E. G. D., and Boys, C. W. G. (1994) Crystal structure of the extracellular region of human tissue factor, *Nature 370*, 662−666.
20. Muller, Y. A., Ultsch, M. H., Kelley, R. F., and de Vos, A. M. (1994) Structure of the extracellular domain of human tissue factor: Location of the factor VIIa binding site, *Biochemistry 33*, 10864−10870.
21. Muller, Y. A., Ultsch, M. H., and de Vos, A. M. (1996) The crystal structure of the extracellular domain of human tissue factor refined to 1.7 Å resolution, *J. Mol. Biol. 256*, 144−159.
22. Semisotnov, G. V., Rodionova, N. A., Razgulyaev, O. I., Uversky, V. N., Gripas, A. F., and Gilmanshin, R. I. (1991) Study of the "molten globule" intermediate state in protein folding by a hydrophobic fluorescent probe, *Biopolymers 13*, 119−128.
23. Myers, J. K., Pace, C. N., and Scholtz, J. M. (1995) Denaturant *m* values and heat capacity changes: Relation to changes in accessible surface areas of protein unfolding, *Protein Sci. 4*, 2138−2148.
24. Naiki, H., Higuchi, K., Hosokawa, M., and Takeda, T. (1989) Fluorometric determination of amyloid fibrils *in vitro* using the fluorescent dye, thioflavin T, *Anal. Biochem. 177*, 244−249.
25. Khurana, R., Ionescu-Zanetti, C., Pope, M., Li, J., Nielson, L., Ramirez-Alvarado, M., Regan, L., Fink, A. L., and Carter, S. A. (2003) A general model for amyloid fibril assembly based on morphological studies using atomic force microscopy, *Biophys. J. 85*, 1135−1144.
26. London, J., Skrzynia, C., and Goldberg, M. E. (1974) Renaturation of *Escherichia coli* tryptophanase after exposure to 8 M urea. Evidence for the existence of nucleation centers, *Eur. J. Biochem. 47*, 409−415.
27. Hammarström, P., Persson, M., Freskgård, P. O., Mårtensson, L. G., Andersson, D., Jonsson, B. H., and Carlsson, U. (1999) Structural mapping of an aggregation nucleation site in a molten globule intermediate, *J. Biol. Chem. 274*, 32897−32903.
28. Litvinovich. S. V., Brew, S. A., Aota, S., Akiyama, S. K., Haudenschild, C., and Ingham, K. C. (1998) Formation of amyloid-like fibrils by self-association of a partially unfolded fibronectin type III module, *J. Mol. Biol. 280*, 245−258.
29. Buxbaum, J. N. (2003) Diseases of protein conformation: What do *in vitro* experiments tell us about *in vivo* diseases? *Trends Biochem. Sci. 11*, 585−592.
30. Mumford, A. D., O'Donnell, J., Gillmore, J. D., Manning, R. A., Hawkins, P. N., and Laffan, M. (2000) Bleeding symptoms and coagulation abnormalities in 337 patients with AL-amyloidosis, *Br. J. Haematol. 110*, 454−460.
31. Choufani, E. B., Sanchorawala, V., Ernst, T., Quillen, K., Skinner, M., Wright, D. G., and Seldin, D. C. (2001) Acquired factor X deficiency in patients with amyloid light-chain amyloidosis: Incidence, bleeding manifestations, and response to high-dose chemotherapy, *Blood 97*, 1885−1887.

BI047388L